13th ewtec 2019 Proceedings of the 13th European Wave and Tidal Energy Conference 1-6 Sept 2019, Naples, Italy

Experimental visualisation of heave plate flow regimes

Curtis J. Rusch, Brian L. Polagye and Benjamin D. Maurer

Abstract—**Two-body point absorber wave energy converters utilize the reaction force between a surface float and inertial mass for power generation. Often, this inertia is produced by the hydrodynamics of a heave plate. Asymmetric heave plates may offer increased stability and favourable hydrodynamics when compared with flat plates, but the intricacies of their hydrodynamics are not well understood. To provide more accurate information for modelling wave energy converters and developing control strategies, we provide an in-depth study of the hydrodynamic force across a wide range of Keulegan-Carpenter numbers, indicative of operational to extreme sea conditions. Primarily, using dye visualization and load cell measurements force, we experimentally demonstrate the connection between fluid phenomena and hydrodynamic force in pure heave. We find that vortex growth is often correlated with variations in force, and often occurs near the peak forces. We also note key features of the hydrodynamic force time series, observing a higher proportion of time spent near peak force during tests indicative of normal operating conditions, and a linear change in force during the down stroke during tests representative of extreme conditions. We extend our observations of the flow field around the heave plate and correlated forces at the load cell to form the basis of recommendations for two-body point-absorber wave energy converter design and control.**

Keywords—**Wave Energy Converters, Point Absorbers, Heave Plates, Flow Visualization, Hydrodynamic Regimes.**

I. Introduction

HEAVE plates have been used in many point absorber wave energy converters (WECs) in recent years. These reaction bodies provide the resistance required for electricity generation from a power-take-off (PTO). Given knowledge of heave plate hydrodynamics, these components may reduce mooring requirements, decrease cost, and enhance survival in storms.

Although many heave plate designs exist, many of those in use with flexibly tethered systems exhibit some form of asymmetry. Since a compliant tether cannot be forced down in the water column by WEC control action, this asymmetry may generate reduced hydrodynamic forces on the down stroke, limiting snap loading. The geometry also leads to higher stability as the heave plate sinks, limiting undesirable side to side motion.

Much of the prior research on heave plates stems from the oil and gas industry, which utilize flat plates to damp the motion of offshore platform spars. This literature covers a wide variety of plate parameters, such as plate porosity [1], edge shape [2], and distance from seabed and surface [3].

Additional work has analysed the flow structures present around oscillating plates, working to link hydrodynamic coefficients with phenomenological structures in the flow. Experimental and numerical study of these flow structures often point toward vortices as key features [4-6]. These studies link plate geometry to vortex behaviour, which, in turn, has implications for the bulk force coefficient response.

A review by Graham [7] notes changing hydrodynamic behaviour indicating two regions of interest. Below a critical condition, vortex shedding occurs at a separation point near the edge of the plate, and oscillatory motion causes vortex pairing and convection away from the plate, while above a critical condition, vortices do not pair, but instead are shed and remain staggered as in a vortex street.

Hydrodynamic force is often decomposed by the method of Morison [8] into a damping force, parameterized by the coefficient of drag (C_d), and inertial force, parameterized by the coefficient of added mass (C_a). Variations in these parameters can be related to the Keulegan-Carpenter number (KC number). For pure sinusoidal motion, the KC number can be expressed as

$$KC = \frac{2\pi A}{D} \tag{1}$$

where A represents the amplitude of oscillation, and D represents the heave plate diameter. Further, the critical

This paper (ID # 1533) was submitted to the wave device development and testing track of the 13th European Wave and Tidal Energy Conference. This work was supported by funding from NAVFAC and the National Science Foundation's Graduate Research Fellowship Program.

C. J. Rusch is in Department of Mechanical Engineering at the University of Washington, Seattle, Washington, USA. (e-mail: curusch@uw.edu)

B. D. Maurer is with the University of Washington Applied Physics Laboratory, Seattle, Washington, USA.

B. L. Polagye is with the Department of Mechanical Engineering at the University of Washington, Seattle, Washington, USA.

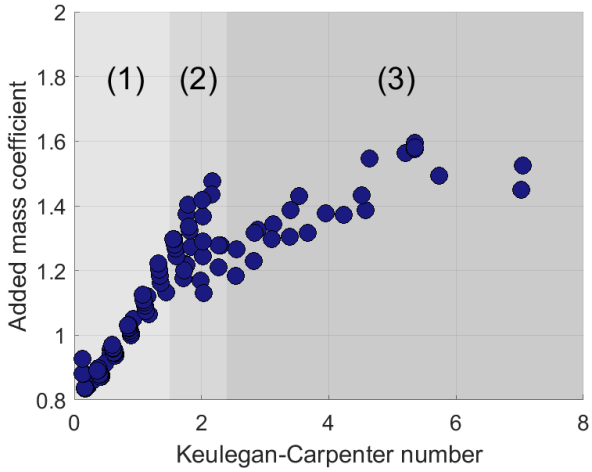

Fig. 1. Scatter plot of C_a vs KC for hexagonal plates of three scales [9]. Three regions of interest are denoted, region (1) covering low KC numbers and consistent hydrodynamics, region (2) is a transitional region, with KC predicting the C_a more weakly, and region (3) covers large KC with a more predictable trend.

transition point identified by Graham [7] can be described in terms of the KC number (of about 20, for their study) for different shaped cylinders and flat plates.

Previously, Rusch et al. extended this body of work to an asymmetric plate of three different sizes, confirming that C_a and C_d scale with KC for asymmetric and symmetric plates [9]. This work involved oscillation of plates across three scales spanning an order of magnitude. Measurement of hydrodynamic force is used to calculate the coefficients of drag and added mass with the Morison equation. Revisiting their results presented in Fig. 1, the trend in C_a across KC illuminates three distinct hydrodynamic regimes: (1) a linear trend of the C_a coefficients at low KC, (2) a bifurcation in the $KC = 1.5 – 2.5$ range, and (3) at $KC > 2.5$, another somewhat linear region appears. Our objective is to explore the relation between phase-average force and fluid phenomena around the heave plates in these three regimes experimentally.

Each of these regions also relate to different regions of operation. KC numbers below 0.7 likely correspond to normal operating conditions for a heave plate connected to a wave-excited component of a point absorber. Most WECs will be optimized for dynamics found in Regime 1. Larger KC cases represent hydrodynamics that occur during larger oscillations produced by storms. Regime 2 may represent typical storm conditions, and heave plates might enter Regime 3 during rare, extreme storms. Understanding hydrodynamic forces across these conditions is critical to WEC survival and efficiency.

II. METHODS

These experiments are carried out in a flow visualization tank. Shown in Fig. 2, the transparent, acrylic tank measures 1.3 x 1.3 meters at its base, stands 1.5 meters tall, and is filled to a volume of approximately 1300 litres. A frame encloses the tank and provides support for a ball-screw linear actuator. This suspends the heave plate from

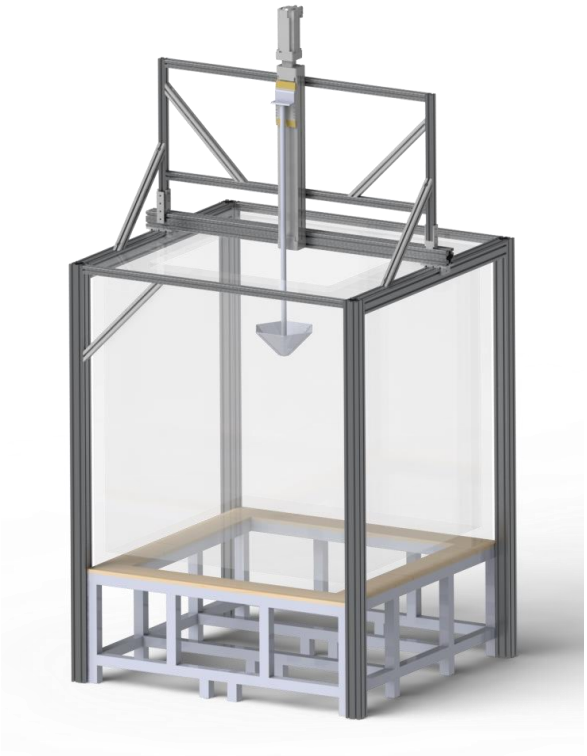

Fig. 2. A computer model of the experimental setup. In practice, the tank is filled with water, and the plate is lowered to mid-water height for testing.

a rod into the water of the tank, and allows a maximum stroke length of 40 cm. A submersible, 6-axis load cell (ATI Mini40) attaches the driving rod to the aluminium hexagonal conic heave plate, which has a diameter of about 0.27 meters. Force produced by the combined effect of the heave plate's inertia, hydrodynamics, weight, and buoyancy are recorded at 1000 Hz.

During experiments, the linear actuator oscillates the plate as a pure sinusoid with a single period and amplitude. Sixteen combinations of period and amplitude were tested, confirming that the results change weakly with period, but more strongly with KC. Here, we discuss in detail three cases that are representative examples of the hydrodynamic forcing and fluid motion found in the three regions denoted in Fig. 1. These cases have parameters of (1) 2 cm amplitude, 1 second period, (2) 6.25 cm amplitude, 1 second period, and (3) 12.9 cm amplitude, 2 second period. Each test consists of seven sinusoidal oscillations, starting from the bottom of the stroke (zero velocity). The plate forces reach steady state after one oscillation, which is excluded from subsequent analyses. After seven oscillations, reflected waves become visually apparent and data collected under these conditions may not be descriptive of unconfined experiments. Between trials the water in the tank is allowed to settle for at least two minutes. The measured force is filtered in post processing with a low-pass IIR filter, using passband and stopband frequencies of 7 and 10 Hz, respectively. Here, we focus solely on the force in the heave direction.

Heave force for each case is presented as a phase average. Hydrodynamic force is calculated from the filtered measurement, $F_{meas.}$ as

$$F_{hydro.} = F_{meas.} - F_{inertia} - F_w + F_b \quad (2)$$

where $F_{hydro.}$ is the hydrodynamic force on the plate, $F_{inertia}$ is the force as a result of plate inertia, F_w is the weight of the plate, and F_b is the buoyancy of the plate. The latter three terms are calculable from plate property, position, and acceleration.

After estimating the hydrodynamic force, each point is binned to a phase in the oscillation (0 to 2π) at a resolution equal to the sampling rate. Data in each bin are then averaged to yield a phase-average hydrodynamic force over one oscillatory period. This force is non-dimensionalized by dividing the phase-averaged force by the root mean square (rms) of the phase-averaged force. The force acting in the downward direction (increasing tension) is defined as positive, and position is defined as positive in the upward direction.

During these experiments, we use dye as a tracer to visualize flow structures at the rim of the heave plate. A piece of 1.5 mm inside diameter Tygon tubing runs from the edge of the tank, down the drive rod to the heave plate. It is fixed to the inside of the plate so that its open end lies just below the inside edge of the plate. Dilute purple food colouring is injected into the tubing via syringe. During experiments, an operator manually compresses the syringe, continuously ejecting dye from the edge of the plate into the flow.

A DSLR camera, recorded video at 60 frames per second. The camera was positioned approximately 2 meters away from one side of the tank on a tripod in the same configuration for all experiments. During recording, two studio lights illuminated the tank from the side against a white Styrofoam backing.

III. RESULTS

We begin by analysing a sequence of images from experiments conducted in each of the three flow regimes. The top row of Figs. 3-5 shows the evolution of the flow around the heave plate at an interval of 1/8th of an oscillation period, T, as compared to the phase-averaged, normalized hydrodynamic force and normalized position (bottom row). Each oscillation starts from the bottom position, rises to its minimum depth, and then returns to bottom.

Fig. 3 is representative of flow Regime 1 (heave plate with a WEC in a typical operating condition). In the flow visualization, we see clear formation and growth of an attached vortex, which remains close to the body of the plate as it rises (frames A-D). This vortex is shed at the apex and, as the plate direction reverses, a vortex begins to form above the plate (frames D-E). Unlike the up stroke, this vortex loses coherence on the down stroke (frames F-G).

At t/T = 0, hydrodynamic force is close to its maximum, then declines to zero when the plate is near mid stroke and at peak velocity (between frames B and C). As the plate reaches its apex and reverses direction, there is a prolonged, maximum compressive force. As with the up stroke, force reversal follows, crossing zero near mid stroke. The maximum compressive and tensile forces plateau in a similar manner on the up and the down stroke, with nearly identical phase lag for the peak force in both directions.

Moving to a larger oscillation amplitude, Fig. 5 presents flow visualization corresponding to a *KC* number that is representative of extreme seas. During the up and down strokes, there are no obvious coherent structures, with the dye illuminating a chaotic wake. At the top and the bottom of the stroke, a vortex forms, but rapidly separates from the plate (frames D-E and H-A). During the period of vortex formation, compressive or tensile forces reach their maximum values and, during periods in which no coherent structures are observable, the time rate of change of the force is relatively constant. The force profile for peak tension and compression differ, as does the location of the shed vortex (frames A and E).

Looking back to a transitional flow representative of Regime 2, Fig. 4 suggests a synthesis of the dynamics present in Regime 1 and Regime 3. Overall, the flow structures are similar to the low *KC* case during the up stroke, but similar to the high *KC* case during the down stroke. Specifically, during the up stroke, a vortex forms beneath the plate, but during the down stroke, the wake is chaotic. During frames A-D, the force is similar to the low *KC* case as well, with an inflection and zero crossing around peak velocity (between B and C), and a peak force (near A) that lags the apex of the stroke. On the down stroke, the peak force occurs earlier and the force profile is nearly linear.

Figures 6 and 7 illustrate these comparisons directly. In Fig. 6, we compare images taken between 0.4 T and 0.6 T at a temporal resolution of 0.025 T for all three representative *KC* numbers. The *KC* = 0.5 (Regime 1) case begins a plateau in the force profile at about t = 0.4 T that extends almost to 0.7 T. On the other hand, for *KC* = 1.5 (Regime 2) and *KC* = 3.0 (Regime 3), the normalized peak compressive forces are larger, and reach a maximum shortly after the stroke apex at 0.5 T. For *KC* = 0.5, the flow structures are nearly stationary except for a small vortex that grows slowly at the top edge of the plate. For *KC* = 3.0, we see a turbulent wake, followed by rapid vortex growth after the reversal of plate direction. Similar to low *KC*, for *KC* = 1.5, the flow structures are initially stationary, then similar to high *KC*, at 0.475 T, a vortex grows quickly above the plate. When that vortex reaches a size similar to the lower vortex, the pair separates from the plate.

Lastly, Fig. 7 compares two other areas of interest for the three regimes. The series of images on the left correspond to 0.1 - 0.2 T. During this period, the force decreases for *KC* = 0.5 and *KC* = 3.0, with no significant change to flow

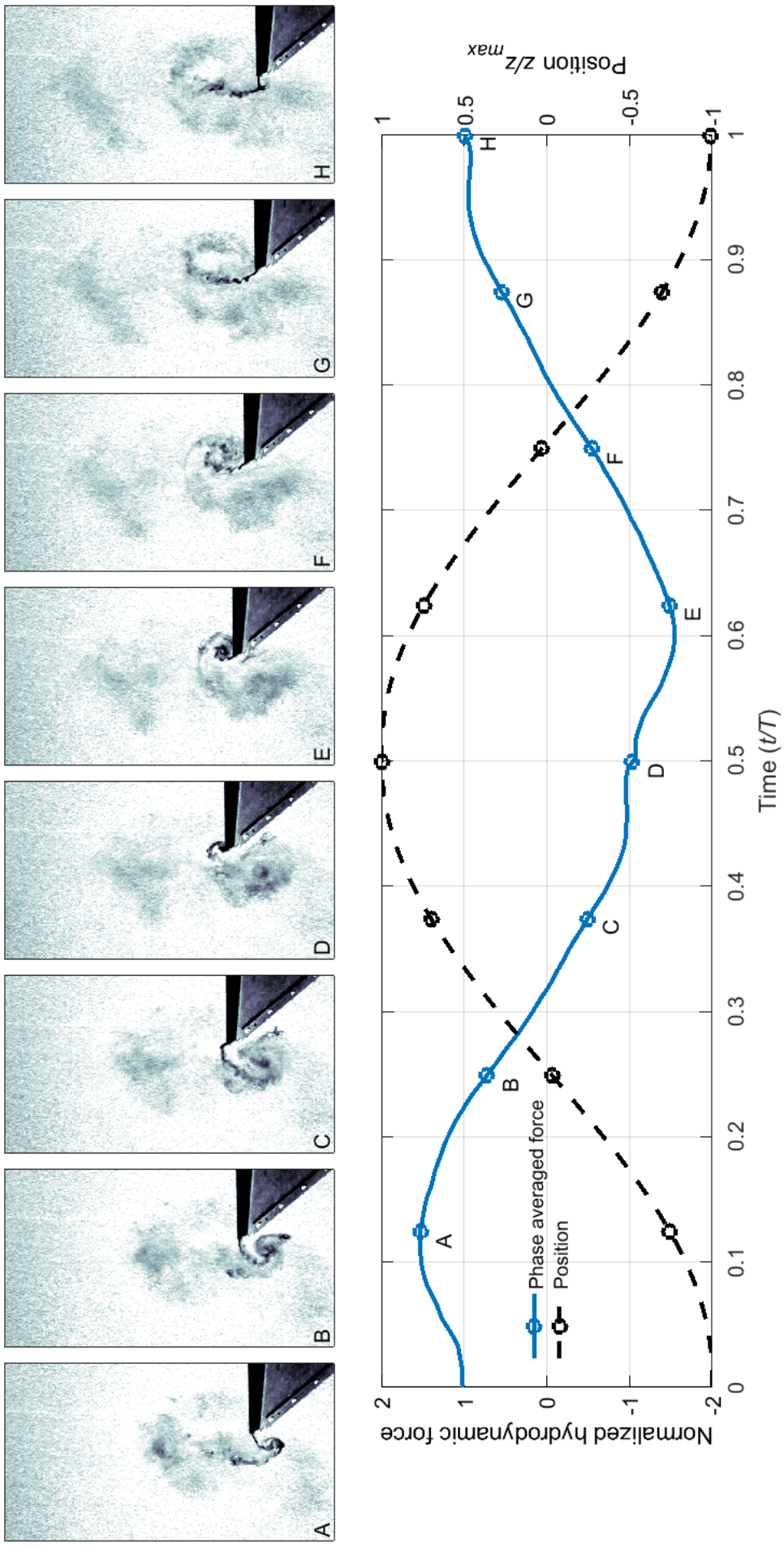

Fig. 3. Visualisation of the flow throughout one oscillation for $KC = 0.5$. Images shown are taken every $1/8^{th}$ of a period. Phase average hydrodynamic force has been nondimensionalized by the rms hydrodynamic force, and position has been nondimensionalized by the maximum position.

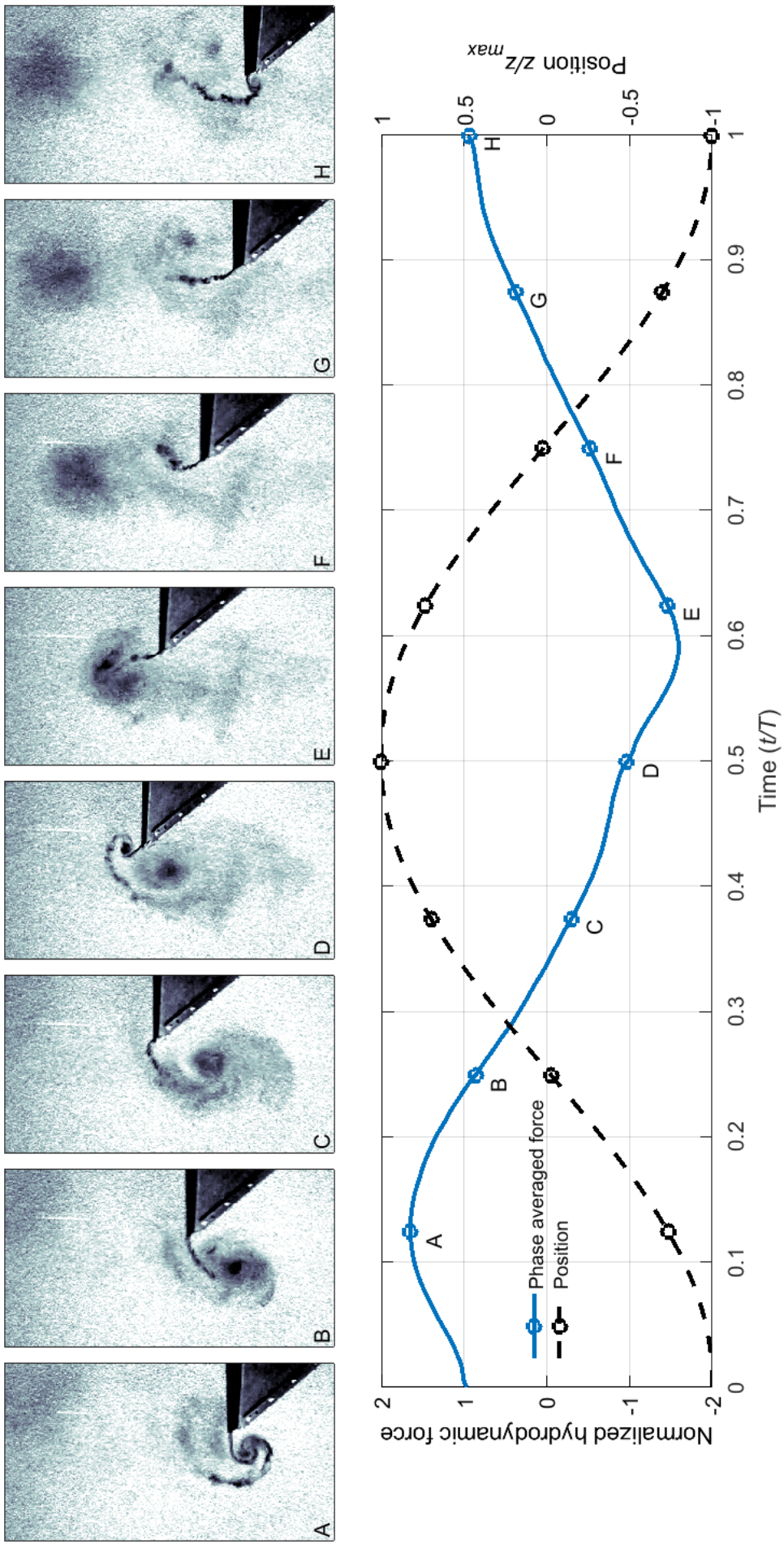

Fig. 4. Visualisation of the flow throughout one oscillation for $KC = 1.5$. Images shown are taken every $1/8^{th}$ of a period. Phase average hydrodynamic force has been nondimensionalized by the rms hydrodynamic force, and position has been nondimensionalized by the maximum position.

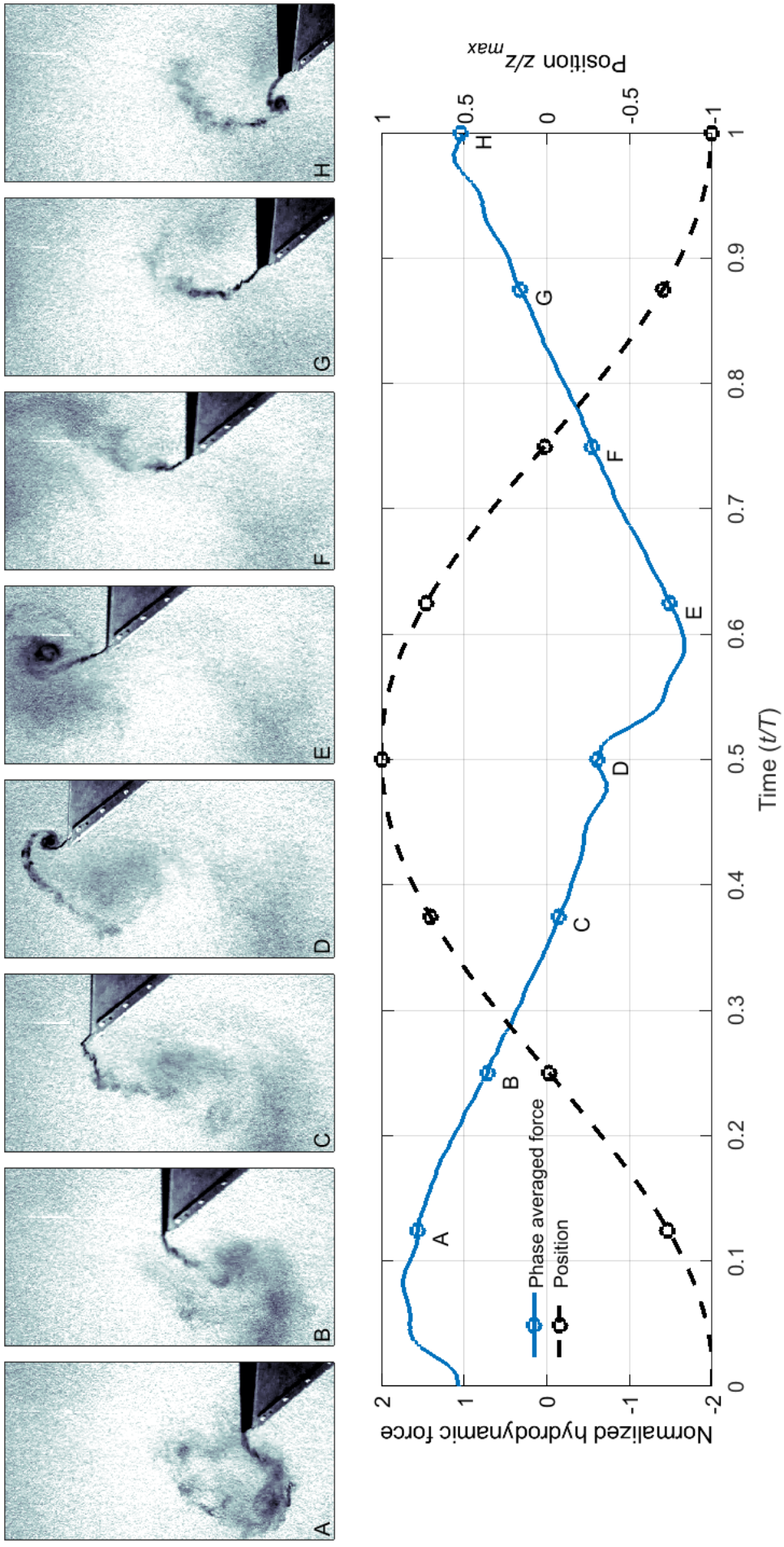

Fig. 5. Visualisation of the flow throughout one oscillation for $KC = 3.0$. Images shown are taken every 1/8th of a period. Phase average hydrodynamic force has been nondimensionalized by the rms hydrodynamic force, and position has been nondimensionalized by the maximum position.

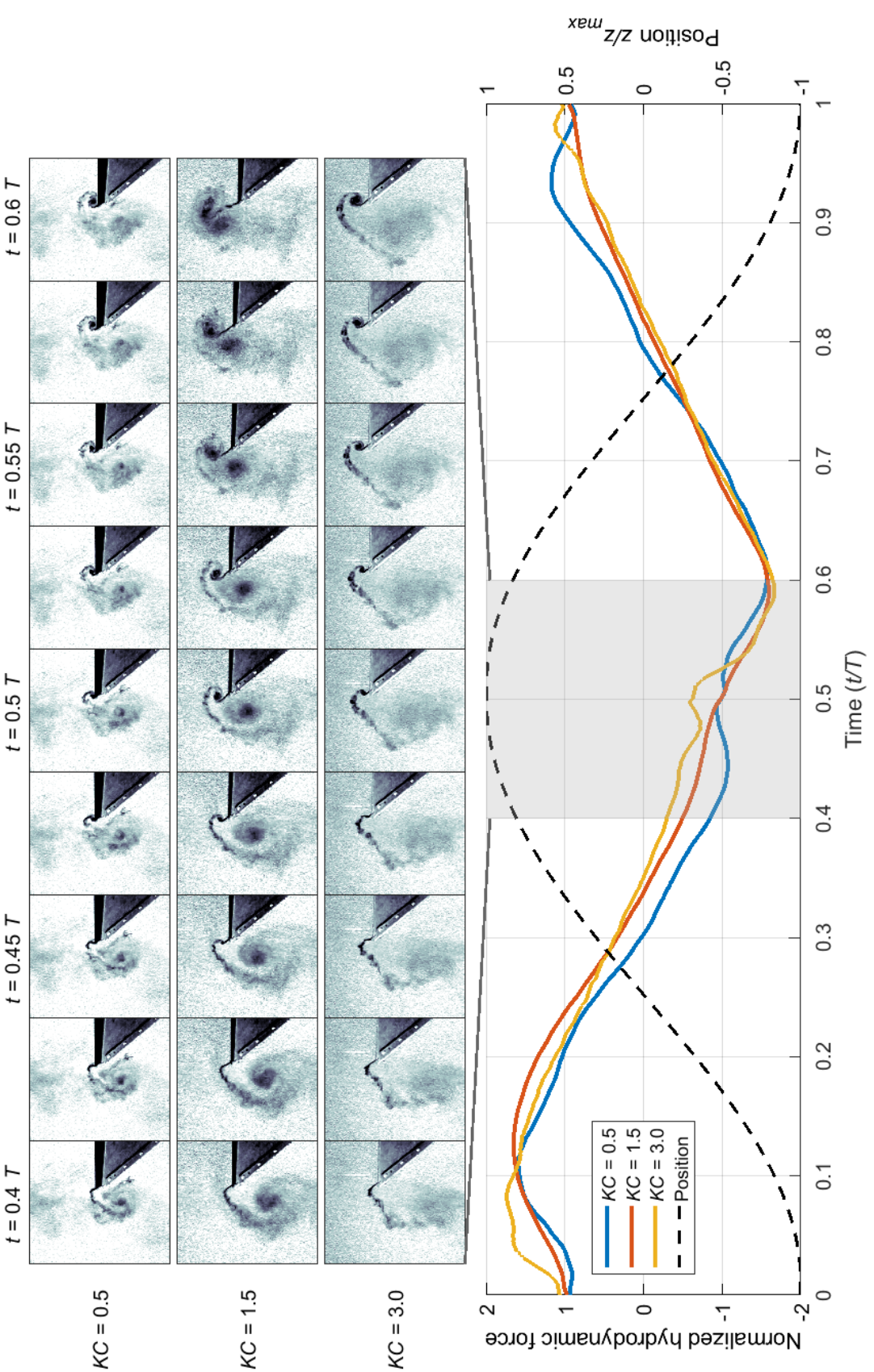

Fig. 6. Image sequence for each of the three representative cases. The images are taken every 1/40th of a period, over the span of time ranging from 2/5th to 3/5th of a period, denoted by the shaded region. The phase-averaged, normalized force is shown for all three regimes, alongside normalized position.

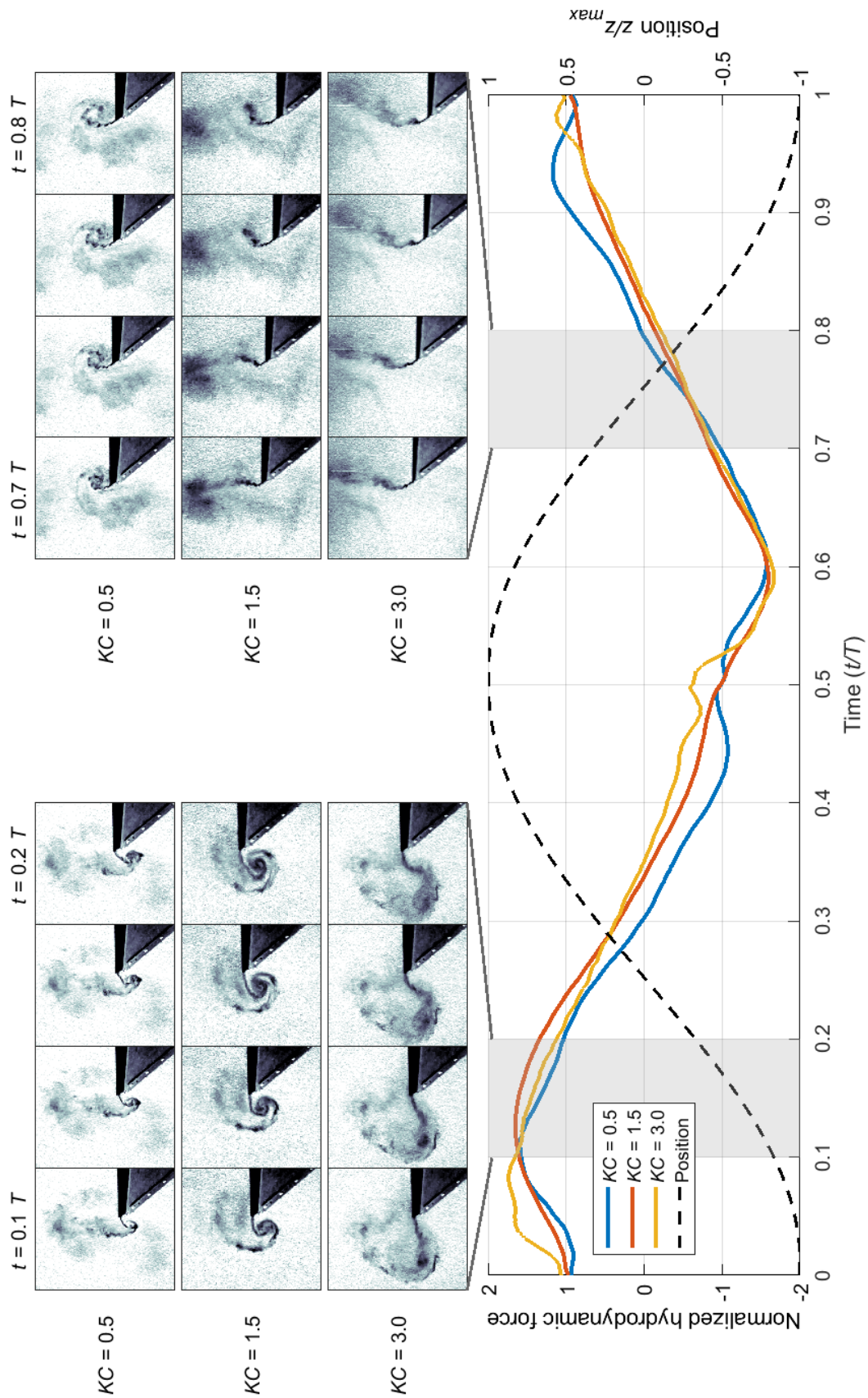

Fig. 7. Image sequence for each of the three representative cases. These images are taken every 1/30th of a period, over two spans ranging from 1/10th to 1/5th of a period, shown on the left, as well as from 7/10th to 4/5th of a period, shown on the right, both regions are shaded for distinction. The phase-averaged, normalized force is shown for all three regimes, alongside normalized position.

structures. On the other hand, at $KC = 1.5$, the force reaches a maximum and a coherent structure rapidly forms.

The set of images on the right correspond to 0.7-0.8 T. For both $KC = 1.5$ and 3.0, the dye stream points almost straight up, suggesting a turbulent wake with no coherent structure. This corresponds to remarkably similar, consistent force profiles through this region for the two cases. On the other hand, the force profile for $KC = 0.5$ changes more rapidly and a vortex grows during this time.

IV. Discussion

Analysing these results in the context of wave energy conversion, we recall that the three cases we have shown are examples of three distinct operating conditions with $KC = 0.5$ representing a normal operating condition, $KC = 1.5$ representing a typical storm condition, and $KC = 3.0$ representing an extreme storm condition.

Starting with comparisons of the three force time series, Fig. 6 and Fig. 7, the variation in the force profile across conditions would likely change the WEC system response. During the normal operating condition example, the force is near the extremes of compression and tension for proportionally more of the stroke. This may have beneficial implications for wave energy conversion, since it would be forgiving if there was a phase mismatch between the force expected by a controller and the actual force imposed by the heave plate.

The force profiles for an example of storm conditions may also be beneficial. During the down stroke (the right half of the force profile), both of the representative storm conditions have linear, consistent force profiles. This would suggest that it should be possible to accurately predict loads on a WEC from the heave plate during the down stroke, allowing for a more accurate prediction of slack loading events. For larger KC, the shape of the force profile approaches that of a saw wave, perhaps providing better load predictability on the up stroke for the most extreme wave conditions. This change in shape is likely a result of the changing balance between forces arising from drag and added mass, as added mass plays a dominant role for low KC, but drag is increasingly important as oscillation amplitude increases.

Negative consequences of these two storm cases may also be observed. The force maxima at both extremes are of short duration for both cases, especially so for the $KC = 3.0$ case, which could increase the mechanical stress on the system.

While dye injection provides only a qualitative snapshot of some of the coherent structures present around the plate, we observe a correlation between vortex structure and the changes in the heave force. For example, in Fig. 7, both of the highlighted regions have cases with no significant vortex growth, and one case with an elevated force co-temporal with rapid vortex growth. Though it is likely that separated flow or the differing volumes of accelerated fluid moving past the plate contribute to the differences in the hydrodynamic force, there is some characteristic of the flow that allows strong vortex growth during regions of extreme or varying force. This is to say that correlation should not be conflated with causation, but this appears to be a useful diagnostic method.

These qualitative results provide a set of conditions to target for future testing. Changes could be made to heave plate geometry in an attempt to alter or control the flow, perhaps through changes in edge shape, strategically placed pressure relief holes in the plate walls, or geometric deformation. Regardless of the link between vortex dynamics and heave force, the dynamics shown in the time series of hydrodynamic force could also inform WEC control strategies and designs for storm conditions. Finally, the changes in phase, shape, and width of the peak force across the three flow regimes are important to take into account for WEC control. Further work with quantitative methods, such as particle image velocimetry (PIV), is required to more fully understand the flow field and the basis for the hydrodynamic forces experienced by the plate.

Acknowledgement

The authors would like to thank Robert Cavagnaro for development of the oscillator and its control software. Additional thanks to Adam Brown, for his original work building up the first oscillator and control system. Further acknowledgement goes to Corey Crisp, and all the members of the Marine Renewable Energy Lab, for their helpful thoughts and feedback.

References

[1] L. Tao, and D. Dray, "Hydrodynamic performance of solid and porous heave plates," *Ocean Eng.*, vol. 35, pp. 1006-1014, 2008.

[2] J. Li, S. Liu, M. Zhao, and B. Teng, "Experimental investigation of the hydrodynamic characteristics of heave plates using forced oscillation," *Ocean Eng.*, vol. 66, pp. 82-91, 2013.

[3] C. A. Garrido-Mendoza, K. P. Thiagarajn, A. Sourto-Iglesias, B. Couscasse, and A. Colagrossi, "Numerical investigation of the flow features around heave plates oscillating close to a free surface or seabed," *33rd Int. Conf. on Ocean, Offshore and Arctic Eng.*, ASME, 2014.

[4] J. S. McNowan and G. H Keulegan, "Vortex formation and resistance in periodic motion," *Journal of Engineering Mechanics Division*, vol 85, pp. 1-6, 1959.

[5] L. Tao and K. Thiagarajan, "Low KC flow regimes of oscillating sharp edges I. Vortex shedding observation," *Applied Ocean Research*, vol. 25, no. 1, pp. 21-35, 2003.

[6] C. A. Garrido-Mendoza, K. P. Thiagarajan, A. Souto-Iglesias, A. Colagrossi, and B. Couscasse, "Computation of flow features and hydrodynamic coefficients around heave plates oscillating near a seabed," *Journal of Fluids and Structures*, vol. 59, pp. 406-431, 2015.

[7] J. M. R. Graham, "The forces on sharp-edged cylinders in oscillatory flow at low Keulegan-Carpenter numbers," *J. Fluid Mech.*, vol 97, part 1, pp. 331-346, 1980.

[8] J. R. Morison, M. P. O'Brien, J. W. Johnson, and S. A. Schaaf, "The force exerted by surface waves on piles," *Journal of Petroleum Technology*, vol. 189, pp. 149–154, 1950.

[9] C. J. Rusch, B. D. Maurer, T. R. Mundon, A. Stewart, and B. Polagye, "Hydrodynamics and scaling of heave plates for point absorbing wave energy converters," in *Proceedings of 12th*

European Wave and Tidal Energy Conference, Cork, Ireland, 2017,
pp. 1-8.